Molecular heterogeneity of CD30$^+$ peripheral T-cell lymphoma with prognostic significance and therapeutic implications: a retrospective multi-centre study

Yu-Jia Huo,[a,o] Shu Cheng,[a,o] Hong-Mei Yi,[b,o] Ting Niu,[c,o] Lei Fan,[d,o] Guo-Hui Cui,[e] Fu-Ling Zhou,[f] Xian-Min Song,[g] Fei Li,[h] Ou Bai,[i] Xiao-Jing Yan,[j] Jun Shi,[k] Ming-Ci Cai,[a] Yao-Hui Huang,[a] Lei Dong,[b] Jie Xiong,[a] Song Hu,[a,l] Yu-Ran Qiu,[a] Yan Zhao,[a] Peng-Peng Xu,[a] Li Wang,[a,m] Min Lu,[a] Hong-Mei Jing,[n,p,**] and Wei-Li Zhao[a,m,p,*]

[a]Shanghai Institute of Hematology, State Key Laboratory of Medical Genomics, National Research Center for Translational Medicine at Shanghai, Ruijin Hospital Affiliated to Shanghai Jiao Tong University School of Medicine, Shanghai, China
[b]Department of Pathology, Shanghai Ruijin Hospital, Shanghai Jiao Tong University School of Medicine, Shanghai, China
[c]Department of Hematology, West China Hospital, Sichuan University, Chengdu, China
[d]Department of Hematology, Pukou CLL Center, The First Affiliated Hospital of Nanjing Medical University, Nanjing, China
[e]Institute of Hematology, Union Hospital, Tongji Medical College, Huazhong University of Science and Technology, Wuhan, China
[f]Department of Hematology, Zhongnan Hospital of Wuhan University, Wuhan, China
[g]Department of Hematology, Shanghai General Hospital, Shanghai Jiao Tong University School of Medicine, Shanghai, China
[h]Center of Hematology, The First Affiliated Hospital of Nanchang University, Nanchang, China
[i]Department of Hematology, First Hospital of Jilin University, Jilin, China
[j]Department of Hematology, First Hospital of China Medical University, Shenyang, China
[k]Department of Hematology, Shanghai Ninth People's Hospital, Shanghai Jiao Tong University School of Medicine, Shanghai, China
[l]School of Life Sciences and Biotechnology, Shanghai Jiao Tong University, Shanghai, China
[m]Pôle de Recherches Sino-Français en Science du Vivant et Génomique, Laboratory of Molecular Pathology, Shanghai, China
[n]Department of Hematology, Lymphoma Research Center, Peking University Third Hospital, Beijing, China

eBioMedicine
2025;115: 105693
Published Online xxx
https://doi.org/10.1016/j.ebiom.2025.105693

Summary

Background Peripheral T-cell lymphoma (PTCL) represents a highly heterogeneous group of non-Hodgkin's lymphomas, often with aggressive biological behaviour. CD30 serves as a pivotal surface antigen in PTCL, however, its biological functions and therapeutic potential warrant further investigation.

Methods We analysed 415 de novo patients with PTCL including 314 in the training cohort and 101 in the validation cohort across 11 medical centres in China. Genomic and transcriptomic profiles were examined by DNA- and RNA-sequencing in 355 and 169 patients, respectively.

Findings In both cohorts, CD30$^+$ PTCL presented significantly increased frequencies of *SETD2*, *STAT3*, and *PTPRS* mutations. Therefore, three molecular subtypes with distinct biological signatures were identified, including the HMA subtype characterised by dysregulation of histone methylation and acetylation, the JNE subtype by alterations in JAK-STAT, Notch signalling pathway, and EBV infection, and the PCT subtype by mutations in phosphorylation, chromatin remodelling, and T-cell receptor-major histocompatibility complex interaction, with extracellular matrix enrichment. Clinically, the JNE subtype demonstrated inferior progression-free survival (PFS) and overall survival (OS), as compared to the HMA and PCT subtypes. Brentuximab vedotin (BV)-containing treatment was associated with improved PFS and OS in the JNE and PCT subtypes. Furthermore, gene expression profile analysis demonstrated underlying vulnerabilities for the HMA, JNE, and PCT subtypes to epigenome-targeting agents, JAK or PI3K inhibitors, and PD-1 inhibitors, respectively.

Interpretation The molecular subtypes of CD30$^+$ PTCL demonstrated prognostic significance and varied sensitivity to BV treatment. Our findings further elucidated molecular regulatory networks of CD30$^+$ PTCL, providing potential co-targeted approaches for genotype-guided precision medicine in PTCL.

*Corresponding author. Shanghai Institute of Hematology, State Key Laboratory of Medical Genomics, National Research Centre for Translational Medicine at Shanghai, Ruijin Hospital Affiliated to Shanghai Jiao Tong University School of Medicine, Shanghai, 200025, China.
**Corresponding author. Department of Hematology, Lymphoma Research Centre, Peking University Third Hospital, Beijing, 100191, China.
E-mail addresses: zhao.weili@yahoo.com (W.-L. Zhao), hongmeijing@bjmu.cn (H.-M. Jing).
[o]These authors contributed equally.
[p]These authors contributed equally.

Funding This study was supported by National Key R&D Program of China, National Natural Science Foundation of China, Clinical Research Plan of Shanghai Hospital Development Centre, Shanghai Clinical Research Centre for Cell Therapy, Shanghai Municipal Health Commission, and China Postdoctoral Science Foundation.

Keywords: Peripheral T-cell lymphoma; CD30; Molecular subtype; Microenvironment; Targeted therapy; Brentuximab vedotin

Research in context

Evidence before this study

PTCL is a malignant proliferation of mature T-lymphocytes often with aggressive clinical course and dismal clinical outcomes. CD30 serves as an important phenotypic marker of PTCL, however, its biological functions and therapeutic potential warrant further investigation. Although BV-CHP is recommended as the first-line therapeutic option for CD30$^+$ PTCL, there still exists clinical unmet to improve the response rate and long-term survival, prompting us to explore the additional biological vulnerabilities of this heterogeneous entity.

Added value of this study

To the best of our knowledge, this is the largest multi-omics analysis on CD30$^+$ PTCL utilising both a training cohort and an external validation cohort across 11 medical centres in China. We have provided comprehensive insights into this molecularly heterogeneous entity, identified and validated three molecular subtypes-HMA, JNE, and PCT-with distinct biological characteristics and differing clinical prognoses. Moreover, survival analysis showed BV-containing treatment was associated with improved PFS and OS in the JNE and PCT subtypes and gene expression profile analysis revealed underlying vulnerabilities for the HMA, JNE, and PCT subtypes to epigenome-targeting agents, JAK or PI3K inhibitors, and PD-1 inhibitors, respectively.

Implications of all the available evidence

The current study not only provided large-scale resource data of this relatively uncommon disease, but also illustrated the benefit of integrating multiple omics data to better understand the relationship between biological and clinical behaviours of CD30$^+$ PTCL. These findings underscore the importance of genotype-guided precision medicine, providing potential co-targeted approaches with BV treatment in PTCL.

Introduction

Peripheral T-cell lymphoma (PTCL) is a highly heterogeneous group of non-Hodgkin's lymphoma derived from mature T-lymphocytes.[1] Anaplastic large-cell lymphoma (ALCL), nodal T-follicular helper cell lymphoma (nTFHL), and PTCL-not otherwise specified (NOS) are the most frequent subtypes within PTCL. Except for anaplastic lymphoma kinase (ALK)-positive ALCL, other nodal PTCL exhibit dismal outcomes upon treatment with standard cyclophosphamide, doxorubicin, vincristine, and prednisolone (CHOP)-based chemotherapy.[2–4]

CD30, encoded by *TNFRSF8*, is a 120-kd transmembrane cytokine receptor of the tumour necrosis factor receptor superfamily and serves as an important phenotypic marker of PTCL.[5] Histologically, CD30 is uniformly expressed in ALCL and varies from 24% to 58% in nTFHL and 23%–64% in PTCL-NOS, respectively.[6,7] Functionally, CD30 confers a survival advantage to the lymphoma cells and mediates tumour microenvironment through various signalling pathways.[8] Our previous study identified three molecular subtypes according to CD30 in DLBCL, including the NM subtype, characterised by dysregulations in nuclear factor Kappa-B (NF-κB) signalling pathway and methylation, with high CD4$^+$ T and follicular helper T (Tfh) cell infiltration; the JA subtype, associated with mutations in Janus kinase (JAK)- signal transducer and activator of transcription (STAT) signalling pathway and acetylation, with high dendritic cell infiltration; and the IB subtype, marked by activation of the B-cell receptor (BCR)- mitogen-activated protein kinase (MAPK) pathway and suppression of immune response.[9] As for CD30 in PTCL, nucleophosmin-ALK fusion is the oncogenic driver in ALK$^+$ ALCL.[10] *TYK2* fusions, as well as *JAK1* and *STAT3* activating mutations, were frequently observed and proved oncogenic in ALK$^-$ ALCL and cutaneous CD30$^+$ T-cell lymphoproliferative disease (CD30$^+$ LPD).[11,12] Additionally, dual specificity phosphatase 22 (*DUSP22*) and *TP63* fusions may serve as prognostic markers in ALK$^-$ ALCL, with *DUSP22* rearrangements potentially indicating the absence of JAK/STAT surrogate markers.[13,14] Gene expression profile highlights that T-cell receptor (TCR)-proximal tyrosine kinases, T-cell differentiation and activation are downregulated in CD30$^+$ PTCL.[15,16] Despite these progress made, biological function of CD30 with therapeutic implications warrant further investigation in PTCL.

Brentuximab vedotin (BV), an anti-CD30 monoclonal antibody-drug conjugate, has exhibited remarkable efficacy in CD30$^+$ PTCL when combined with chemotherapy, as shown in the ECHELON-2 trial.[17,18] However, post hoc analysis failed to detect the correlation between CD30 expression levels and treatment response, and other clinical studies showed that patients with elevated CD30 expression may not experience significant benefits from BV treatment.[19,20] To address this, we conducted an integrated analysis of clinicopathologic, genomic, and transcriptomic analysis in a multi-centre cohort of 418 de novo PTCL. Our study uncovered three molecular subtypes of CD30$^+$ PTCL with prognostic significance and varied sensitivity to BV treatment. Furthermore, distinct biological signatures and vulnerabilities of these subtypes may suggest potential co-therapeutic strategies in the era of precision medicine in PTCL.

Methods

Ethics

The retrospective study was approved by the Shanghai Ruijin Hospital Institutional Ethics Review Board (No. 2018-167) and informed consent was obtained in accordance with the Declaration of Helsinki. Ten other medical centres in China within the cooperative network of the Multicentre Haematology-Oncology Programs Evaluation System (M-HOPES) including Peking University Third Hospital, West China Hospital, First Affiliated Hospital of Nanjing Medical University, Union Hospital, Zhongnan Hospital, Shanghai General Hospital, First Affiliated Hospital of Nanchang University, First Hospital of Jilin University, First Hospital of China Medical University, and Shanghai Ninth People's Hospital have accepted the decision of the Ethics Review Board of Shanghai Ruijin Hospital.

Patients

As the training cohort, 314 de novo patients with PTCL including 44 ALK$^+$ ALCL (14.0%), 39 systemic ALK$^-$ ALCL (12.4%), 153 nTFHL (48.7%, including 145 nTFHL-angioimmunoblastic-type [nTFHL-AI] and 8 nTFHL-NOS), and 78 PTCL-NOS (24.8%) were enrolled from Shanghai Ruijin Hospital between January 2013 and July 2023. Additionally, 101 de novo patients with PTCL were recruited from other ten medical centres during the same period, comprising 9 ALK$^+$ ALCL (8.9%), 4 systemic ALK$^-$ ALCL (4.0%), 56 nTFHL (55.4%, including 51 nTFHL-AI and 5 nTFHL-NOS), and 32 PTCL-NOS (31.7%) as the validation cohort (Fig. 1a). All patients were Asian and their sex was obtained from clinical health records.

Histological diagnoses were reviewed in accordance with the 5th WHO classification and international consensus classification from the clinical advisory committee, and independently confirmed by two expert pathologists (H.-M Yi and L. Dong).[2,3] All patients had available immunohistochemistry results for CD30 and clinical parameters in international prognostic index (IPI). The majority of the patients (88.0%) received anthracycline-containing regimens, with or without etoposide, while other patients (12.0%) received BV-containing treatment. Autologous (auto-) or allogeneic (allo-) hematopoietic stem-cell transplantation (HSCT) was selectively performed based on clinical consensus and patients' intentions, with a total of 52 patients undergoing HSCT.

Immunohistochemistry and chromogenic in situ hybridisation

Immunohistochemistry was performed on 4-μm formalin-fixed paraffin-embedded (FFPE) tissue using indirect immunoperoxidase using the LEICA BOND-III automated staining platform as previously described.[21] CD30 staining was performed using anti-CD30 BerH2 antibody (Cat# GA602, RRID: AB_3675588, DAKO, Danmark) and the protein expression levels were estimated semi-quantitatively (increments of 5%, i.e., 5%, 10%, 15%). CD30 positivity was confirmed when 10% or greater of neoplastic cells (in cases where enumeration of neoplastic cells was not possible, total lymphocytes may have been used) expressed CD30 at any intensity.[17,18] Double staining of PAX5/CD30 were also performed in available tissues to detect the existence of CD30$^+$ large B-cell blasts. The sections were firstly incubated with anti-PAX5 antibody (Cat# GA650, RRID: AB_3678472, DAKO, Danmark) and treated with AEC to produce the visible red-purple pigment. After rinsing, sections were incubated with the second anti-CD30 antibody and treated with DAB to produce the visible brown pigment.

Tfh makers, including BCL6, CD10, CXCL13, ICOS and PD-1 were evaluated during differential diagnosis between nTHFL and PTCL-NOS.[22] At least two positive Tfh markers, including strong PD1 expression, B-immunoblasts, follicular dendritic cell expansion, and RHOA p.G17V or IDH2 p.R172 mutations were considered as the desirable diagnostic criteria to diagnose nTFHL.[3] To distinguish ALK$^-$ ALCL and CD30$^+$ PTCL-NOS, ALK$^-$ ALCL was diagnosed when large lymphoid cells with copious cytoplasm and pleomorphic characteristics with horseshoe-shaped or reniform nuclei. Evading of lymph node sinuses and strong uniform CD30 expression were considered as the desirable diagnostic criteria for ALK$^-$ ALCL.[23]

Chromogenic in situ hybridisation (CISH) for Epstein–Barr virus-encoded RNA (EBER) was performed using an ISH kit (Roche, Switzerland) on FFPE sections using the LEICA BOND-III automated staining platform as previously described.[21] EBER positivity was assessed in total lymphocytes, encompassing both partial and strong positivity, as previously reported.[24,25] In addition, double labeling of EBER-ISH and CD20

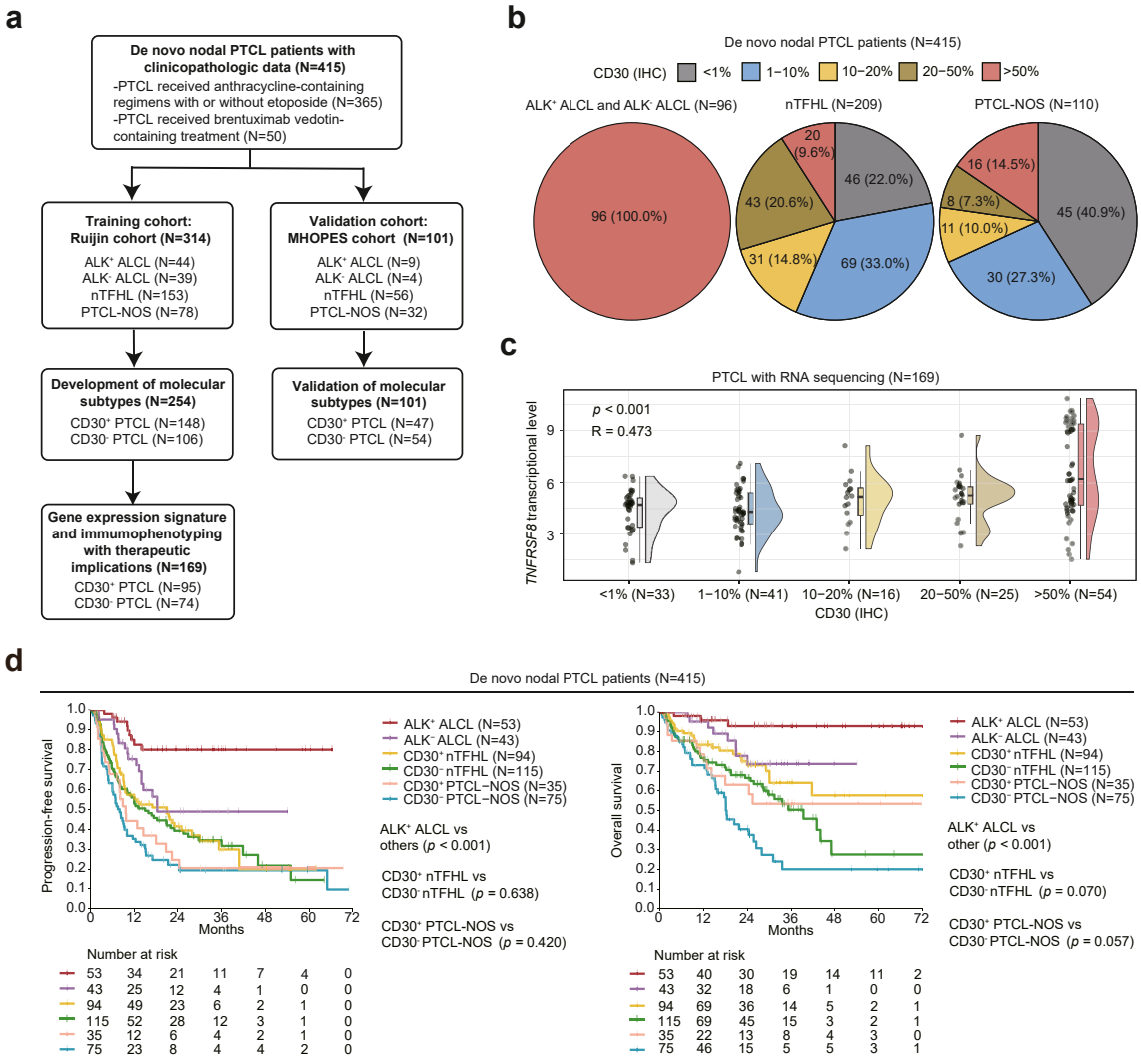

Fig. 1: **Flowchart of the study and survival analysis in PTCL.** (a) Flowchart of cohort selection and exploratory aspects. (b) Semi-quantitative evaluation by IHC of CD30 expression in nTFHL and PTCL-NOS. (c) *TNFRSF8* transcripts by RNA-sequencing among each CD30 expression subgroup by IHC in PTCL. *p*-value was calculated with the Pearson correlation test. (d) Kaplan–Meier curves of progression-free survival (left panel) and overall (right panel) survival according to histological types and CD30 expression. *p*-values were calculated with the log-rank test. IHC, immunohistochemistry.

immunohistochemistry was performed to detect the existence of EBER$^+$ B cells in cases with available tissues. The immunohistochemical demonstration of CD20 antigens (anti-CD20 antibody, Cat# GA604, RRID: AB_3678473, DAKO, Danmark) followed by EBER-ISH was performed under RNase-free condition. EBV-infected B cells became visible by their purple nuclei and brown membrane staining.

DNA sequencing and subtype establishment

For DNA sequencing, 62 whole exome sequencing (WES) and 192 targeted next-generation sequencing (tNGS) data from Shanghai Ruijin Hospital, as well as 101 tNGS data from other MHOPES centres were analysed in this study. Among them, all WES and 95 tNGS data from Shanghai Ruijin Hospital were referred in our previous study.[26] The sequencing and data analysis procedures of WES were consistent with those reported in our previous study.[26] For targeted next-generation sequencing (tNGS), genomic DNA was extracted using a DNeasy Blood & Tissue Kit (Qiagen, Hilden, Germany) according to the manufacturer's instructions. A total of 82 genes were selected from WES data for further study based on two criteria: (i) genes with recurrent mutations (>3%) and/or (ii) genes relevant to pathogenesis of PTCL. Targeted capture sequencing was

performed using established Illumina protocols on novaseq6000 platform. Multiplexed libraries of tagged amplicons from PTCL tumour samples were generated by Shanghai Yuanqi Bio-Pharmaceutical Multiplex-PCR Amplification System.

Overall, non-silent mutations were inspected including 1302 nonsynonymous SNV, 95 in-frame deletion or insertion, 298 frameshift deletion, insertion or stop-gain, and 32 splicing in the training cohort and 343 nonsynonymous SNV, 38 in-frame deletion and insertion, 138 frameshift deletion, insertion or stop-gain, and 15 splicing in the validation cohort (Supplementary Table S1). Based on Gene Ontology (GO) and Kyoto Encyclopedia of Genes and Genomes (KEGG) database, candidate genes were assigned to specific biological processes, including chromatin remodelling, DNA methylation, histone methylation, histone acetylation, JAK-STAT signalling pathway, Notch signalling pathway, P53 signalling pathway, phosphorylation, phosphatidylinositol 3-kinase (PI3K)-AKT signalling pathway, Rho GTPase, and TCR-major histocompatibility complex (MHC) interaction (Supplementary Table S2).

The method used to establish molecular subtypes in $CD30^+$ PTCL was similar to the approach described for $CD30^+$ DLBCL.[9] To establish the molecular subtypes, we first identified the *seed genes* including *SETD2*, *STAT3*, and protein tyrosine phosphatase receptor S (*PTPRS*) for each molecular subtype. Subsequently, we screened additional genes and EBER protein based on their correlation with the seed genes in $CD30^+$ PTCL and their involved pathways listed in Supplementary Table S2, to determine the *scoring factors* for each subtype. A total of 24 additional mutated genes and EBER were identified as scoring factors in subtype establishment. When classifying patients, those with the seed genes of a specific subtype were assigned to that subtype. If a patient did not have any seed genes, scores were assigned to each patient based on the scoring factors of the subtypes, with each scoring factor contributing one point. The patient was then assigned to the subtype with the highest score. Importantly, the seed genes and scoring factors of a specific subtype must exhibit the highest frequency of gene mutation or protein expression within their respective subtypes. Few patients could be unclassified due to the absence of relevant scoring factors.

RNA sequencing and bioinformatics analysis

For RNA sequencing (RNA-seq), a total of 169 sequencing data was analysed in this study, including 131 sequencing data referred in our previous study.[26] Extended 38 patients total RNA was extracted from frozen tumour samples of patients using the RNeasy Mini Kit (Qiagen, Hilden, Germany) as previously report. RNA size, concentration, and integrity were verified using Agilent 2100 System (Agilent). RNA libraries were constructed by using VAHTS total RNA-seq (HMR) library prep kit according to the manufacturer's instructions, and sequenced on Illumina NovaSeq 6000 System. Paired-end reads were harvested from Illumina NovaSeq 6000 System, and the quality were controlled by Q30.

Read pairs were aligned to GRCh37 RefSeq by STAR (version 2.5.3a).[27] The HTSeq was applied to generate table files containing transcript counts.[28] R package *sva* (version 3.50.0) to remove the batch effect and R package *limma* (version 3.58.1) was used to normalise the raw reads and obtain differentially expressed genes (DEGs, defined as fold change >1.500 and $p < 0.050$). Transcripts per million (TPM) were generated using Kallisto (version 0.46.0) with default parameters.[29] The original Kallisto outputs were integrated with R package *tximport* (version 1.24.0) and the TPM of all alternative splicing transcripts of a gene were summed to represent the gene expression level. Before gene expression signatures for lymphoma microenvironment and drug sensitivity calculation, log2 transformed TPM data (log_2TPM) were processed with R package *preprocessCore* (version 1.58.0), which implemented the quantile normalisation described before and removed batch effect caused by sequencing time, which confirmed by PCA analysis, with R package *limma* (version 3.58.1).[30]

Gene Set Enrichment Analysis (GSEA) was performed using R package *clusterProfiler* (version 4.10.1) with MSigDB-curated gene sets (c2.cp. kegg.v6.2.symbols.gmt) and (c5.all.v7.1.symbols.gmt).[31] PTCL origins and tumour microenvironmental cells gene sets were extracted from published literature.[30,32] Functional gene expression score (F^{GES}) of PTCL origins and tumour microenvironmental cells were calculated using single sample GESA (ssGESA) algorithm with the R package *GSVA* (version 1.50.5).[33] The Cancer Therapeutics Response Portal (CTRP) V2 was applied to predict the therapeutic response of each patient with PTCL to small-molecules using the R package *oncoPredict* (version 1.2).[34] Each patient's drug sensitivity, linked to detailed genomic information, was estimated by the half-maximal inhibitory concentration (IC50).

Genomic and microenvironment classification of PTCL

Genomic and microenvironment classification of PTCL were identified as described by Huang et al.[26] For 355 patients with DNA sequencing data, patients were assigned to 103 T1, 94 T2, 119 T3.1, and 39 T3.2. For 169 patients with RNA-seq data, hierarchical clustering of the matrix was performed using the R package *pHeatmap* (v 1.0.12) using ward.D2 as linkage, resulting in 59 LME1, 49 LME2, 19 LME3, and 42 LME4.

Cell lines and transfection

The H9, Jurkat, and Karpas-299 were mycoplasma free and independently authenticated by short tandem repeat profiling (Supplementary Table S3). All cell lines were

grown in RPMI-1640 medium, supplemented with 10% heat-inactivated fetal bovine serum and 1% penicillin/streptomycin (15140122, Gibco, Carlsbad, CA, USA) in a humidified atmosphere containing 5% CO_2 at 37 °C.

To overexpress *SETD2*, *STAT3*, and *PTPRS*, pLXT-SFFV-mCherry-BSD (vector), pLXT-SFFV-mCherry-BSD-*SETD2* (NM_014159, wild-type, wt), pLXT-SFFV-mCherry-*SETD2* (NM_01415, G2299R), pLXT-SFFV-GFP-puro-*STAT3* (NM_139276, wild-type, wt), pLXT-SFFV-GFP-puro-*STAT3* (NM_139276, D661Y), pLXT-SFFV-GFP-puro-*PTPRS* (NM_002850, wild-type, wt), pLXT-SFFV-GFP-puro-*PTPRS* (NM_002850, Q1549L) plasmids were constructed. To knockdown *SETD2*, *STAT3*, and *PTPRS*, pLKO5-mCherry-BSD (Scramble), pLKO5-mCherry-BSD-sh*SETD2*, pLKO5-GFP-Puro (Scramble), pLKO5-GFP-Puro-sh*STAT3*, and pLKO5-GFP-Puro-sh*PTPRS* plasmids were constructed. Cell lines were transfected with viral particles containing above purified plasmids using lipofectamine 2000 (11668019, Invitrogen, Carlsbad, CA, USA) according to the manufacturer's protocol (MOI = 50). The stably transduced clones were selected by FITC green or red fluorescence protein using flow cytometry. The shRNA sequences are listed in Supplementary Table S4.

Quantitative real-time PCR (qRT-PCR)

The total RNA was extracted using Trizol reagent and reverse transcribed using a PrimeScript RT Reagent Kit with gDNA Eraser for qRT-PCR (RR047A, TaKaRa, Japan). qRT-PCR was performed using SYBR Premix Ex TaqTM II (RR820A, TaKaRa, Japan) and ABI ViiA7 (Applied Biosystems, Bedford, MA, USA) following the manufacturer's instructions. Relative quantification was calculated using the 2–ΔΔCT methods. The primers are listed in Supplementary Table S5.

Western blot

Cells were lysed in 200 μl lysis buffer (0.5 M Tris–HCl, pH 6.8, 2 mM EDTA, 10% glycerol, 2% SDS, and 5% β-mercaptoethanol). Protein lysates (20 μg) were electrophoresed on 10% SDS polyacrylamide gels and transferred to nitrocellulose membranes. Membranes were blocked with 5% non-fat dried milk and incubated overnight at 4 °C with the appropriate primary antibodies, followed by a horseradish peroxidase-conjugated secondary antibody. The immunocomplexes were visualized using a chemiluminescence phototope-horseradish peroxidase Kit (Cell Signalling Technologies, Danvers, MA, USA). The antibodies were validated and listed in Supplementary Table S3.

Flow cytometry

The antibody used for testing CD30 was PE anti-CD30 (Cat# 550041, RRID: AB_393541, BD Biosciences, USA). Flow cytometry data were collected by a FACS Calibur cytometer (BD Biosciences), and the median fluorescent intensity (MFI) was analysed using FlowJo software (version 10.8.1).

Statistical analysis

The Fisher's exact test was used to compare categorical variables. For normally distributed data, comparisons between groups were made using the Student's t-test. In cases where the data did not follow a normal distribution, the Mann–Whitney U test was used for comparing two groups, and the Kruskal–Wallis test was applied for comparisons involving three groups. Pearson correlation coefficients were used to evaluate the correlation between variates. Progression-free survival (PFS) was measured from the date of diagnosis to the date when disease progression/relapse was recognized or the date of the last follow-up. Overall survival (OS) was calculated from the date of diagnosis to the date of death or the date of the last follow-up. Survival functions were estimated using the Kaplan–Meier method and compared using the log-rank test. Univariate and multivariable hazard estimates were generated with Cox proportional hazards model. Covariates with $p < 0.050$ in both PFS and OS of univariate analysis were included in the multivariate model and analysed with the backward Wald method. Statistical significance was defined as $p < 0.050$. All statistical analysis was performed using Statistical Package for the Social Sciences (SPSS) 25.0 (SPSS Inc., Chicago, IL, USA), GraphPad Prism 9, and RStudio (version 4.3.2).

Role of funders

The funders did not have any role in the study design, data collection, data analyses, data interpretation, or writing of the manuscript.

Results

Clinical and pathological characteristics of CD30$^+$ PTCL

Cohort selection and exploratory aspects were outlined in Fig. 1a. Using semi-quantitative immunohistochemistry, both ALK$^+$ ALCL and ALK$^-$ ALCL were characterised by high CD30 expression with CD30 level >50%. In the nTFHL subgroup, 46 (22.0%), 69 (33.0%), 31 (14.8%), 43 (20.6%), and 20 (9.6%) cases showed CD30 level <1%, 1–10%, 10–20%, 20–50%, and >50%, respectively. In the PTCL-NOS subgroup, 45 (40.9%), 30 (27.3%), 11 (10.0%), 8 (7.3%), and 16 (14.5%) cases showed CD30 level <1%, 1–10%, 10–20%, 20–50%, and >50%, respectively. Using a cut-off value of 10%, CD30$^+$ PTCL accounted for 45.0% and 31.8% of PTCL in the nTFHL and PTCL-NOS subgroups, respectively (Fig. 1b). Semi-quantitative immunohistochemistry of CD30 was significantly correlated with *TNFRSF8* transcriptional level by RNA-seq in PTCL ($R = 0.473$, $p < 0.001$, Pearson correlation test; Fig. 1c). CD30/PAX5

double staining was performed on 22 cases of nTFHL, 4 cases of PTCL-NOS, and 4 cases of ALCL. None of the PTCL-NOS or ALCL cases exhibited double-positive staining. Among the 22 nTFHL cases, 10 (45%) showed double-positive cells, while the remaining 12 (55%) exhibited only CD30 single-positive cells. In the 10 double-positive cases, the proportion of such cells ranged from 5% to 50% (Supplementary Fig. S1a).

In the training cohort, with a median follow-up of 27.5 months, the 2-year PFS and OS rates were 42.6% (95% CI 36.5–48.7) and 65.3% (95% CI 59.4–71.2), respectively. In the validation cohort, with a median follow-up of 20.0 months, the predictive 2-year PFS and OS rates were 37.3% (95% CI 25.9–48.7) and 74.8% (95% CI 63.8–85.8), respectively. No significant differences in PFS and OS were observed between the training and validation cohorts (Supplementary Fig. S2a and b). Pathologically, ALK$^+$ ALCL exhibited a 2-year PFS rate of 80.1% (95% CI 68.3–91.9) and a 2-year OS rate of 89.5% (95% CI 85.2–100.0), which were significantly better than other PTCL subgroups (all $p < 0.001$, log-rank test). CD30 was not a prognostic predictor for PFS or OS neither in the nTFHL nor in the PTCL-NOS subgroups (Fig. 1d).

The main clinical and pathological characteristics of PTCL according to CD30 expression were summarized in Supplementary Table S6. Patients with CD30$^+$ PTCL were significantly more likely to have young age ($p = 0.010$), good performance status ($p = 0.011$), early Ann Arbor stage ($p < 0.001$), normal Lactate Dehydrogenase level ($p = 0.003$), less bone marrow involvement ($p = 0.012$), and low-risk IPI score ($p < 0.001$, all Fisher's exact test) compared to those with CD30$^-$ PTCL. However, no significant differences were observed between patients with CD30$^+$ PTCL and CD30$^-$ PTCL within the nTFHL and PTCL-NOS subgroups. In addition, patients with CD30$^+$ PTCL in the PTCL-NOS subgroup were significantly more likely to be EBER-positive than those with CD30$^-$ PTCL ($p = 0.042$, Fisher's exact test). For the double-labeling of EBER-ISH and CD20 immunohistochemistry, a total of 10 cases were analysed, including 8 nTFHL and 2 PTCL-NOS cases. All 8 nTFHL cases displayed double-positive cells. Among the 2 PTCL-NOS cases, 1 (50%) exhibited double-positive cells, while the other (50%) presented only EBER single-positive cells (Supplementary Fig. S1b).

Genomic and transcriptomic analysis of CD30$^+$ PTCL

DNA sequencing was performed on 355 patients, including 39 ALK$^+$ ALCL (11.0%), 37 ALK$^-$ ALCL (10.4%), 189 nTFHL (53.2%), and 90 PTCL-NOS (25.4%) and separated into the training cohort of 254 cases and the validation cohort of 101 cases. Mutations of candidate genes with annotated biological processes are shown in Fig. 2a and Supplementary Table S7. The mutational landscape of CD30$^+$ PTCL displayed an enrichment in ALCL, which fitted the pathobiology of ALK$^+$ ALCL and ALK$^-$ ALCL, as previously reported.[32,35] In the training cohort, CD30$^+$ PTCL had higher frequencies in *SETD2* (11.5% vs. 3.8%, $p = 0.036$), *NOTCH2* (10.1% vs. 1.9%, $p = 0.010$), *STAT3* (9.5% vs. 1.9%, $p = 0.017$), and *PTPRS* (9.5% vs. 1.9%, $p = 0.017$) mutations, along with lower frequencies in *TET2* (49.3% vs. 64.2%, $p = 0.015$), and *VAV1* (2.7% vs. 8.5%, $p = 0.047$, all Fisher's exact test) mutations than CD30$^-$ PTCL (Fig. 2b). In the validation cohort, *SETD2* (12.8% vs. 1.9%, $p = 0.048$), *STAT3* (12.8% vs. 1.9%, $p = 0.048$), and *PTPRS* (12.8% vs. 0.0%, $p = 0.008$, all Fisher's exact test) mutations were also more frequent in CD30$^+$ PTCL than in CD30$^-$ PTCL (Fig. 2b).

Mutant sites of *SETD2*, *STAT3*, and *PTPRS* in patients with CD30$^+$ PTCL are illustrated in Supplementary Figure S3a. Preclinical models were constructed based on the expression of *SETD2*, *STAT3*, *PTPRS*, and *TNFRSF8* in H9, Jurkat and Karpas-299 cell lines (Supplementary Fig. S3b). *SETD2*^{wt}, *SETD2*^{G2299R}, as well as *STAT3*^{kd} and *PTPRS*^{kd}, were established and transfected into the H9 cells. Meanwhile, *STAT3*^{wt}, *STAT3*^{D661Y}, *PTPRS*^{wt}, *PTPRS*^{Q1549L}, as well as shRNA to knockdown *SETD2*^{kd}, were established and transfected into the Jurkat cells. Western blot analysis confirmed the transfection efficiency (Supplementary Fig. S3c–e). Total CD30 expression was upregulated in *SETD2*^{G2299R}, compared to *SETD2*^{wt}, with a similar pattern in *PTPRS*^{kd}, compared to scramble and downregulated in *STAT3*^{kd}, compared to scramble H9 cells (Fig. 2c, upper panel). On the other hand, total CD30 expression was upregulated in *SETD2*^{kd} compared to scramble, with a similar pattern in *STAT3*^{D661Y} compared to vector, and *PTPRS*^{Q1549L}, compared to *PTPRS*^{wt} Jurkat cells (Fig. 2c, lower panel). Moreover, CD30 expression on tumour cell membrane revealed by flow cytometry confirmed the above results (Supplementary Fig. S4a–f). Together, these data demonstrated that functional loss of *SETD2* and *PTPRS*, as well as functional gain of *STAT3*, contributed to increased CD30 expression in T-lymphoma cell models.

RNA-seq was further analysed in 169 patients, including 22 ALK$^+$ ALCL (13.0%), 14 ALK$^-$ ALCL (8.3%), 98 nTFHL (58.0%), and 35 PTCL-NOS (20.7%). Three hundred and eight-five upregulated differentially expressed genes (DEGs), including *BATF3*, *RUNX2*, *SP8*, as translational factors, and 683 downregulated DEGs were identified in 95 CD30$^+$ PTCL cases, compared with 74 CD30$^-$ PTCL cases (Supplementary Table S8). As revealed by GSEA, extracellular matrix structural constituent, fibroblast growth factor receptor signalling, Hedgehog signalling, Notch receptor process, and response to tumour growth factor (TGF)-β were significantly upregulated, while processes including B-cell activation, CCR and CXCR chemokine receptor, T-cell activation, and T-cell mediated immunity were significantly downregulated in CD30$^+$ PTCL (Supplementary Fig. S5a). As for PTCL origin, CD30$^+$

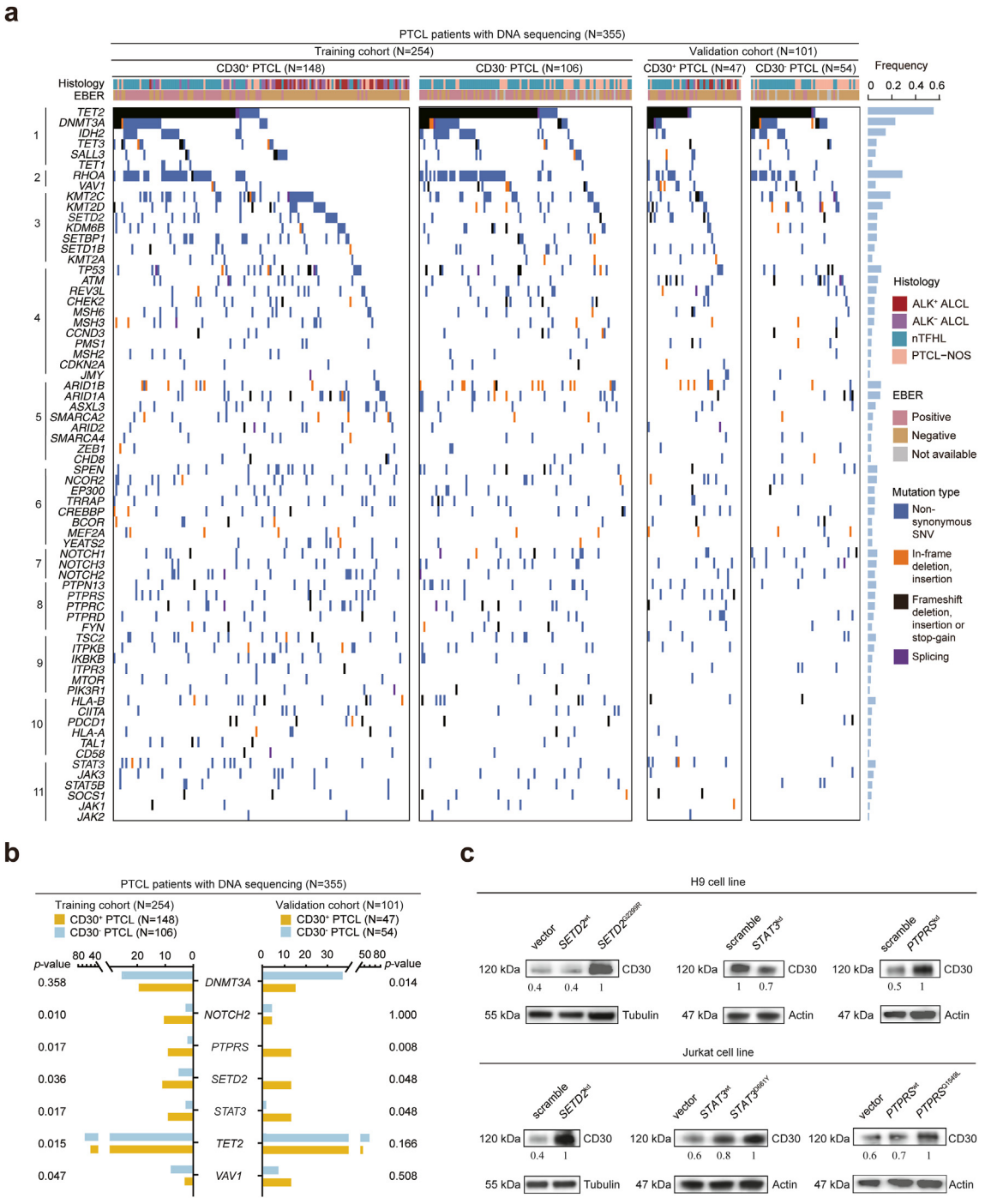

***Fig. 2:* Genomic analysis in PTCL according to CD30 expression**. (a) Waterfall plot of mutations of 68 candidate genes according to CD30 expression between patients with $CD30^+$ PTCL and $CD30^-$ PTCL in the training and validation cohorts. Functional clusters of the candidate genes are indicated at left: 1, DNA methylation; 2, Rho GTPase; 3, histone methylation; 4, P53 signalling pathway; 5, chromatin remodelling; 6, histone acetylation; 7, Notch signalling pathway; 8, phosphorylation; 9, PI3K-AKT signalling pathway; 10, T-cell receptor-major histocompatibility complex; 11, JAK-STAT signalling pathway. The column represents each patient with histological types and EBER expression. (b) Gene mutations with significant differences between patients with $CD30^+$ PTCL and $CD30^-$ PTCL in the training and validation cohorts along with the *p*-value for the distribution. *p*-values were calculated using the Fisher's exact test. (c) Total CD30 expression of tumour cells detected in H9 (upper panel) and Jurkat cell lines (lower panel) transfected with subtype-specific *SETD2*, *STAT3*, and *PTPRS* lentiviruses, respectively, by Western blot.

PTCL harbored a significantly increased score of functional genes representing ALCL, but a decreased score of Tfh and PTCL-NOS-TBX21 (all $p < 0.001$, Mann–Whitney U test; Supplementary Fig. S5b).

Molecular subtypes of CD30$^+$ PTCL

Based on the aforementioned results, *SETD2*, *STAT3*, and *PTPRS*, representing three significant molecular alterations in CD30$^+$ PTCL, were defined as the seed genes to form the three molecular subtypes. The schema diagram of CD30$^+$ PTCL molecular subtyping was illustrated in Supplementary Fig. S6a. Genes associated with histone methylation and acetylation (*KMT2A*, *KMT2C*, *KMT2D*, *SETD2*, *SETD1B*, *BCOR*, *CREBBP*, and *NCOR2*) were selected as the scoring factors for the HMA subtype. Additionally, genes involved in the JAK-STAT and Notch signalling pathways (*JAK3*, *SOCS1*, *STAT3*, *STAT5B*, *NOTCH1*, and *NOTCH2*), along with EBER were included in the JNE subtype, while genes related to phosphorylation, chromatin remodelling, and TCR-MHC interaction (*PTPN13*, *PTPRC*, *PTPRS*, *ARID1A*, *ARID1B*, *ARID2*, *ASLX3*, *SMARCA2*, *HLA-B*, and *TAL1*) were selected for the PCT subtype (Fig. 3). Overall, 136 out of 148 (91.9%) CD30$^+$ PTCL in the training cohort and 43 out of 47 (91.5%) CD30$^+$ PTCL in the validation cohort were classified into three molecular subtypes including the HMA subtype (56 cases), JNE subtype (62 cases), and PCT subtype (61 cases). Detailed percentages of certain scoring factors in the training, validation, and overall cohorts were illustrated in Supplementary Fig. S6b–d. The molecular subtypes also remained valid with the same seed genes and scoring factors in nodal PTCL except for ALK$^+$ ALCL (Supplementary Fig. S6e).

No significant differences were observed among the three molecular subtypes in the aspect of histological types, semi-quantitative immunohistochemistry of CD30, and clinical parameters (Supplementary Fig. S6f and g, Supplementary Table S9). As for the genomic aspect, CD30$^+$ PTCL harbored more T3.1 than CD30$^-$ PTCL ($p = 0.002$, Fisher's exact test), with the HMA subtype harboring the highest percentage of T3.1 ($p = 0.033$, Fisher's exact test) and the PCT subtype harboring the highest percentage of T3.2 ($p = 0.009$, Fisher's exact test; Supplementary Fig. S7a and b).

Clinical and prognostic significance of molecular subtypes of CD30$^+$ PTCL

In the training cohort of classified 136 patients with CD30$^+$ PTCL, the 2-year PFS rates for the HMA, JNE, and PCT subtypes were 62.1%, 33.4%, and 53.7%, and the 2-year OS rates for the HMA, JNE, and PCT subtypes were 90.6%, 61.5%, and 81.3%, respectively. Three molecular subtypes differed significantly in PFS and OS, with poorer prognosis in the JNE subtype than the HMA subtype ($p = 0.003$ for PFS, $p = 0.001$ for OS, log-

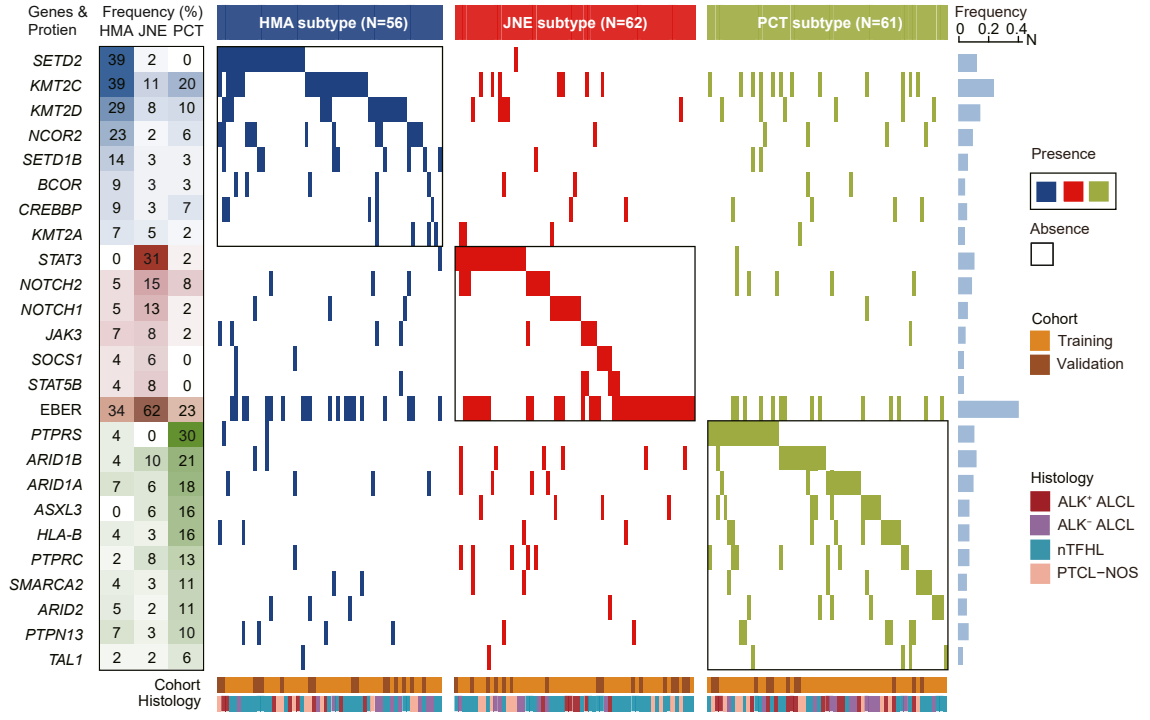

***Fig. 3:* Genetic features of molecular subtypes of CD30$^+$ PTCL.** Genetic composition in the HMA (upper panel), JNE (middle panel), and PCT (lower panel) subtypes. The prevalence of the indicated genetic mutations and EBER was indicated at the left. The column represents each patient with histological types.

rank test) and the PCT subtype (p = 0.008 for PFS, p = 0.013 for OS, log-rank test; Fig. 4a). In the validation cohort of classified 43 patients with CD30$^+$ PTCL, the predictive 2-year PFS rates for the HMA, JNE, and PCT subtypes were 32.1%, 22.5%, and 65.6%, and the predictive 2-year OS rates for the HMA, JNE, and PCT subtypes were 100%, 69.2%, and 100%, respectively. Three molecular subtypes also showed significant differences in PFS and OS, with poorer prognosis in the JNE subtype than the HMA subtype (p = 0.048 for PFS, p = 0.030 for OS, log-rank test) and the PCT subtype (p = 0.018 for PFS, p = 0.037 for OS, log-rank test; Fig. 4b).

Due to relatively limited number of the patient for each cohort, univariate and multivariate models were constructed between clinicopathological factors, treatment interventions, and molecular subtypes of CD30$^+$ PTCL in the overall cohort. The JNE subtype was strongly related to inferior PFS (p < 0.001, Cox proportional hazards model) and OS (p < 0.001, Cox proportional hazards model) and recognized as an independent adverse prognostic factor for both PFS (hazard ratio [HR] = 3.299, 95% CI 2.137–5.092, p < 0.001, Cox proportional hazards model) and OS (HR = 4.807, 95% CI 2.356–9.807, p < 0.001, Cox proportional hazards model) when IPI risk group was controlled (Table 1).

Transcriptomic analysis of molecular subtypes of CD30$^+$ PTCL

As revealed by RNA-seq of 89 classified patients with CD30$^+$ PTCL, epigenetic processes, oncogenic signalling pathways, and immune-associated pathways were consistent with the gene mutation profile (Fig. 5a). The HMA subtype (Fig. 5b, upper panel) was mainly involved with aberrant histone methylation and acetylation (*EED*, *HDAC2*, *METTL3*, *SETD4*), as well as cell cycle (*ANAPC7*, *MYC*, *SSBP1*, *TP63*) processes. The JNE subtype (Fig. 5b, middle panel) was mainly involved with upregulated JAK-STAT (*IL-27RA*, *JAK3*, *STAT3/5A*), Notch (*DLL1*, *DTX1*, *NOTCH1/2*), and PI3K-AKT (*PIK3C2B*, *PIK3CD*, *PIK3CG*, *PIK3IP1*) signalling pathways. The PCT subtype (Fig. 5b, lower panel) was mainly involved with dysregulated extracellular

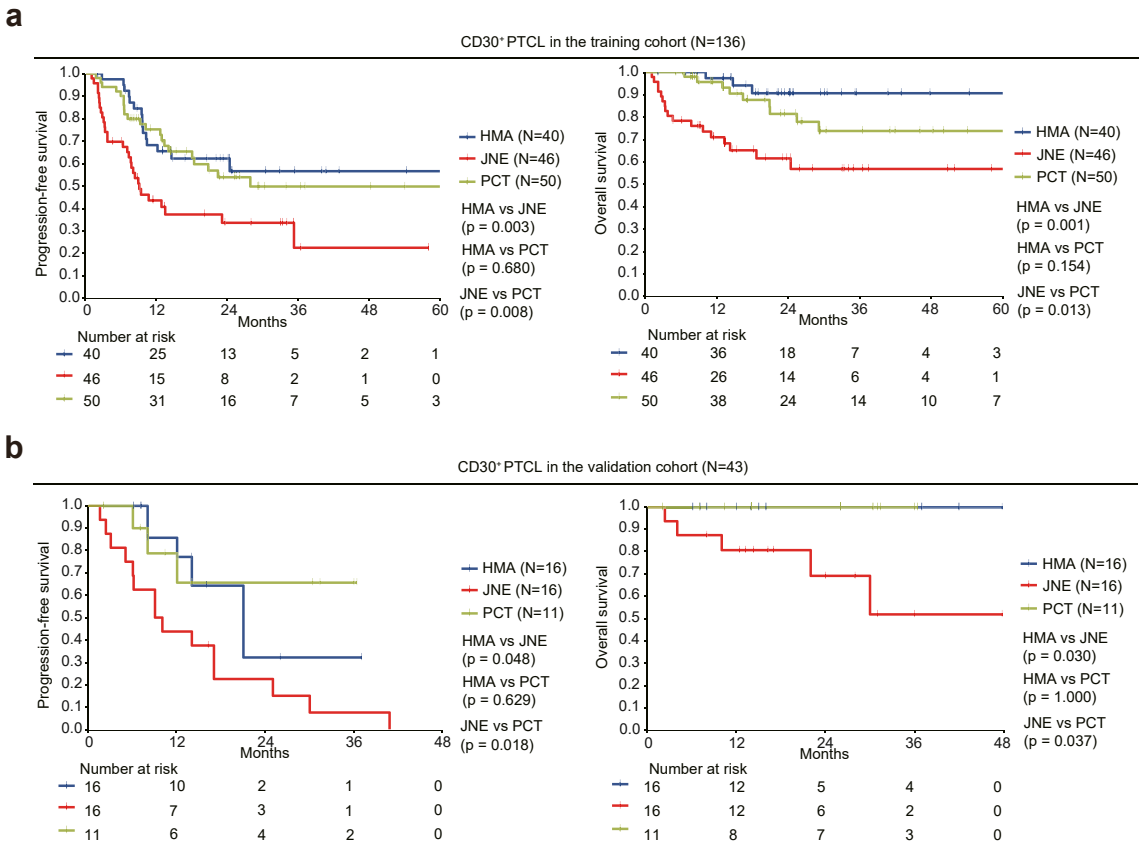

***Fig. 4:* Survival analysis in CD30$^+$ PTCL according to molecular subtypes.** Kaplan–Meier curves of progression-free survival and overall survival according to molecular subtypes of CD30$^+$ PTCL in the training cohort (a) and the validation cohort (b). *p*-values were calculated with the log-rank test.

Risk factors	Univariate analysis				Multivariate analysis			
	PFS		OS		PFS		OS	
	p-value	HR (95% CI)	*p*-value	HR (95% CI)	*p*-value	HR (95% CI)	*p*-value	HR (95% CI)
Histology	0.001		0.066					
Non-ALK$^+$ ALCL		Reference		Reference				
ALK$^+$ ALCL		0.257 (0.112–0.588)		0.034 (0.001–1.253)				
IPI risk group	<0.001		0.003		<0.001		<0.001	
Low		Reference		Reference		Reference		Reference
Low-intermediate		1.692 (0.846–3.383)		4.106 (0.871–19.365)		1.541 (0.769–3.085)		3.549 (0.752–16.744)
Intermediate-high		2.674 (1.390–5.141)		5.595 (1.236–25.317)		3.101 (1.606–5.989)		5.742 (1.269–25.983)
High		4.151 (2.113–8.155)		12.455 (2.797–55.461)		5.282 (2.653–10.514)		13.902 (3.108–62.183)
BV treatment	0.050	0.589 (0.346–1.001)	0.014	0.165 (0.040–0.690)				
HSCT	0.164	0.680 (0.395–1.171)	0.060	0.320 (0.098–1.048)				
HMA subtype	0.030	0.582 (0.357–0.950)	0.007	0.197 (0.060–0.645)				
JNE subtype	<0.001	2.613 (1.722–3.966)	<0.001	4.314 (2.132–8.728)	<0.001	3.299 (2.137, 5.092)	<0.001	4.807 (2.356, 9.807)
PCT subtype	0.033	0.601 (0.376–0.960)	0.200	0.607 (0.283–1.303)				

Abbreviations: ALCL, anaplastic large-cell lymphoma; ALK, anaplastic lymphoma kinase; BV, brentuximab vedotin; CI, confidence interval; HR, hazard ratio; HSCT, hematopoietic stem-cell transplantation; IPI, international prognostic index; OS, overall survival; PFS, progression-free survival. *p*-values were calculated with the Cox proportional hazards model.

Table 1: **Univariate and multivariate analysis for progression-free survival and overall survival in CD30$^+$ peripheral T-cell lymphoma.**

regulated kinase (ERK)/fibroblast growth factor (FGF) signalling pathway (*FGF12/7*, *HTRA1*, *SP8*), chromatin remodelling (*CENPH*, *CENPL*, *CENPW*), and extracellular matrix (ECM) structural organization (collagen type I alpha 2 [*COL1A2*], hyaluronan Synthase [*HAS*] *1/2*, laminin Beta 4 [*LAMB4*]). As for lymphoma microenvironment (LME), CD30$^+$ PTCL showed a higher percentage of mesenchymal subtype, compared to CD30$^-$ PTCL (p = 0.048, Fisher's exact test; Supplementary Fig. S7c and d). Considering cellular and non-cellular stromal components, the PCT subtype was significantly associated with higher cancer-associated fibroblasts (CAFs) (p = 0.044, t-test), and the HMA subtype was significantly associated with lower ECM (p = 0.045, Mann–Whitney U test) and lymphatic endothelial cells (p = 0.030, t-test; Fig. 5c). Overall, a schematic description of specific driver mutations, distinct gene expression profiles, and tumour microenvironment patterns in three molecular subtypes of CD30$^+$ PTCL was illustrated in Fig. 5d.

Therapeutic implications of molecular subtypes of CD30$^+$ PTCL

We first analysed the efficacy of the front-line BV-containing treatment in molecular subtypes of CD30$^+$ PTCL. ALK$^+$ ALCL was excluded due to notably better survival and unbalanced proportion between non-BV and BV treatment to control confounding bias. In the HMA subtype, BV treatment had no statistical survival benefit (Fig. 6a). Nevertheless, BV treatment demonstrated significantly better PFS and OS than non-BV treatment in the JNE (p = 0.019 for PFS, p = 0.046 for OS, log-rank test; Fig. 6b) and the PCT subtypes (p = 0.023 for PFS, p = 0.037 for OS, log-rank test; Fig. 6c). Functional analysis related to BV response showed significant upregulated adaptive immune response (p = 0.004) and complement activation (p = 0.040) in the JNE subtype (Fig. 6d, upper panel) and endoplasmic reticulum lumen (p = 0.001) and response to oxidative stress (p = 0.013, all adjusted by Benjamini & Hochberg) in the PCT subtype (Fig. 6d, lower panel). In addition, we sought other targeted agents for molecular subtypes of CD30$^+$ PTCL. Based on the CTRP database, hypomethylating agents, 5-azacytidine (p = 0.006, t-test), and histone deacetylase (HDAC) inhibitor (p = 0.014, t-test) showed significantly higher efficacy in the HMA subtype (Fig. 6e and f). JAK (p < 0.001, t-test) and PI3K (p = 0.012, t-test) inhibitors were significantly more effective in the JNE subtype (Fig. 6g and h).

Discussion

This is, to our knowledge, the largest multi-omics study on CD30$^+$ PTCL, demonstrating the genomic and transcriptomic pattern of this molecularly heterogeneous entity. More importantly, we identified and validated three molecular subtypes of CD30$^+$ PTCL with distinct biological characteristics and therapeutic implications.

The HMA subtype was mainly based on alterations in histone methylation and acetylation. *SETD2*, the methyltransferase of histone 3 lysine 36 trimethylation, mediates multiple transcriptional-related events in lymphoma progression.[36] *SETD2*, as well as other histone methylation-associated genes including *SETD1B* and *KMT2A/C/D*, are frequently mutated in ALCL and CD30$^+$ LPD, together with histone acetylation-associated genes, mainly as *CREBBP*.[37,38] *KMT2C*, *KMT2D*, and *CREBBP* mutations are also the prominent features of T3.1, contributing to the highest prevalence of T3.1 in

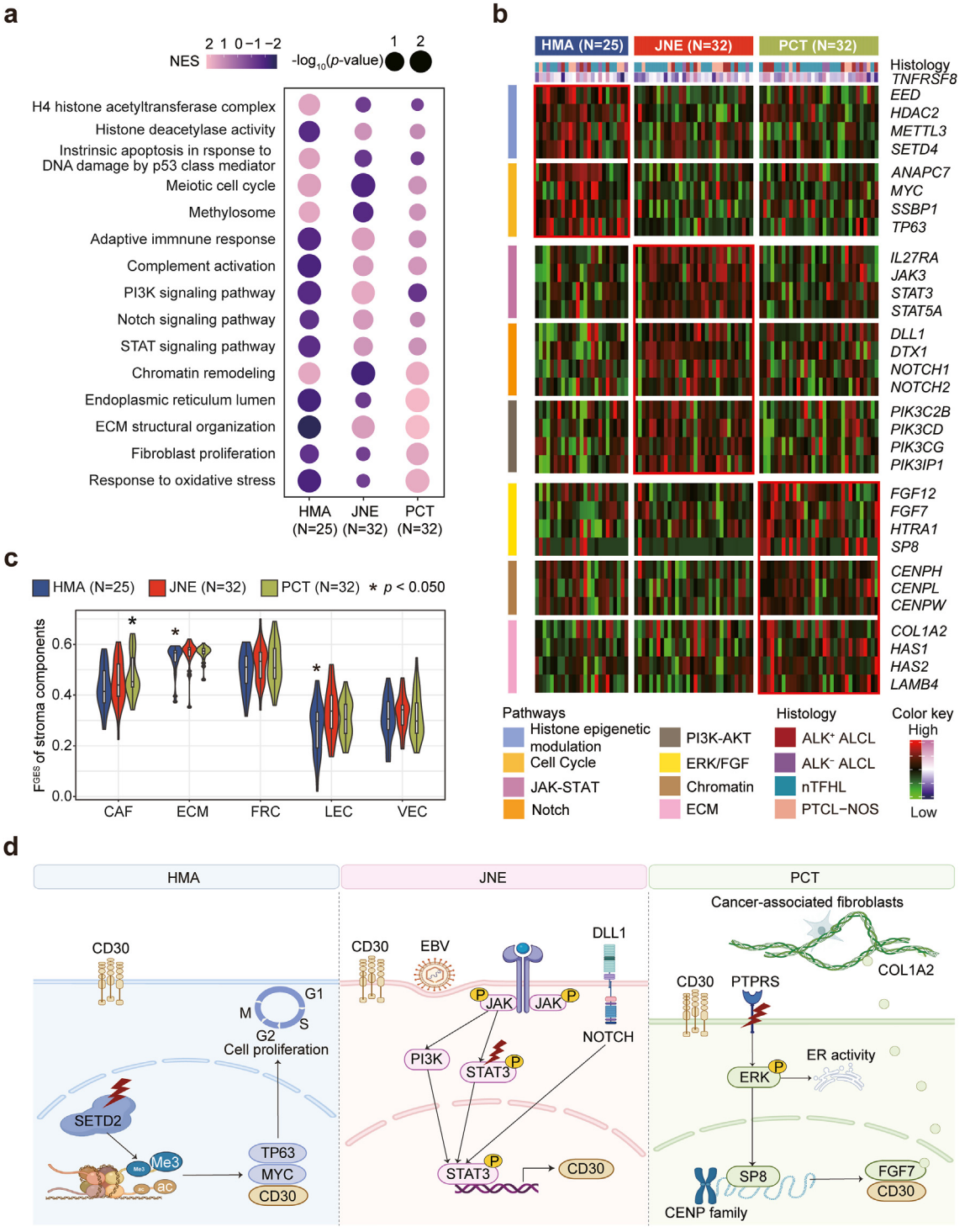

***Fig. 5:* Gene expression signature and lymphoma microenvironment of molecular subtypes of CD30⁺ PTCL.** (a) Epigenetic processes, oncogenic signalling pathways, and immune-associated pathways among three molecular subtypes in CD30⁺ PTCL. *p*-value and normalised enrichment score were calculated between certain molecular subtype vs. other subtypes of CD30⁺ PTCL. (b) Gene expression profiling of main alterations in the HMA (upper panel), JNE (middle panel), and PCT (lower panel) subtypes. Involved pathways are indicated at the left. The column represents each patient with CD30⁺ PTCL with histological types and *TNFRSF8* transcriptional expression. (c) Functional gene expression score of stroma components among three molecular subtypes in CD30⁺ PTCL. *p*-value was calculated between certain molecular subtype vs.

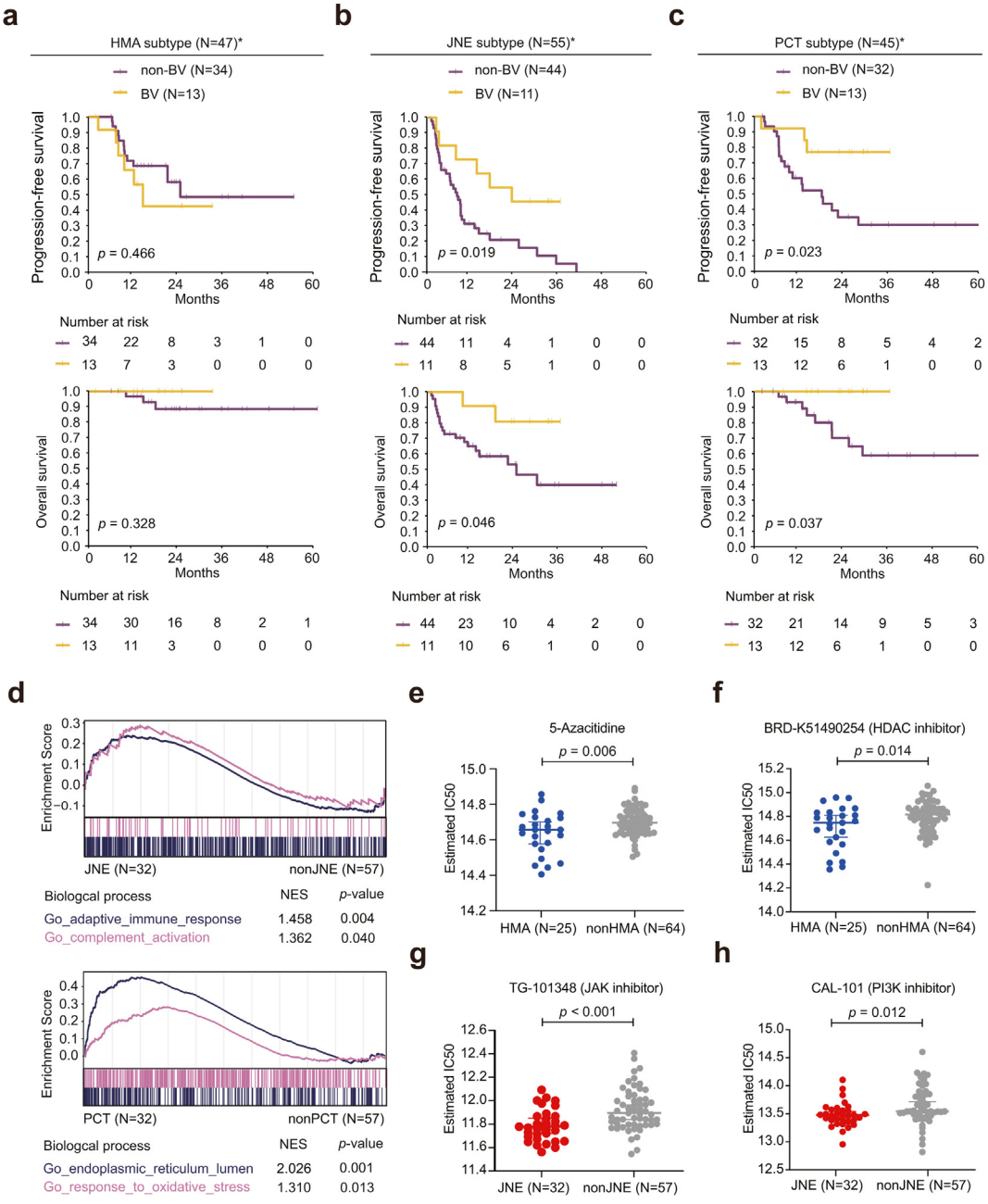

***Fig. 6:* Clinical implications of molecular subtypes of CD30⁺ PTCL.** Kaplan–Meier curves of progression-free survival (upper panel) and overall survival (lower panel) according to BV treatment in the HMA (a), JNE (b), and PCT (c) subtypes. *p*-values were calculated with the log-rank test. (d) Dysregulated pathways related to BV response. *p*-value and normalised enrichment score were calculated between certain molecular subtype vs. other subtypes of CD30⁺ PTCL. (e–h) Estimated half-maximal inhibitory concentration in molecular subtypes of CD30⁺ PTCL. *p*-values were calculated between certain molecular subtype vs. other subtypes of CD30⁺ PTCL using t-test. * ALK⁺ ALCL was excluded in this analysis. BV, brentuximab vedotin; IC50, half-maximal inhibitory concentration.

other subtypes of CD30⁺ PTCL using the Mann–Whitney U test or t-test on the basis of the data distribution. (d) Schematic description illustrating pathogenesis of CD30⁺ PTCL molecular subtypes. Based on genomic and transcriptomic data, three molecular subtypes were identified in CD30⁺ PTCL with specific driver mutations (highlighted with lightening stickers), and distinct gene expression profiles and tumour microenvironment patterns. CAF, cancer-associated fibroblast; ECM, extracellular matrix; ER, endoplasmic reticulum; F^{GES}, functional gene expression score; FRC, fibroblastic reticular cells; LEC, lymphatic endothelial cells; VEC, vascular endothelial cells.

the HMA subtype.[26] As for the gene expression profile, mutations of histone modification genes resulted in dysregulation of epigenetic processes and further influenced cell cycle progression, explaining why TP63 and MYC were highly expressed in the HMA subtype.[39] Regarding therapeutic implications, the hypomethylating agents and HDAC inhibitors are effective in the HMA subtype. 5-Azacytidine treatment improves the effect of standard CHOP in the nTFHL subgroup and integrated analysis indicates that deletion of *SETD2* induced sensitivity to hypomethylating agents.[40,41] Moreover, chidamide, a class I HDAC inhibitor increases response rate in PTCL-NOS with *KMT2D* or *CREBBP* mutations, and another class I HDAC inhibitor romidepsin demonstrates improved PFS in nTFHL, when combined with CHOP.[42,43] Although BV alone did not show a significant survival benefit, preclinical research demonstrates a synergistic effect between BV and chidamide in promoting apoptotic pathways of T-lymphoma cells, suggesting future rationale of combining epigenetic agents with BV to further improve the outcomes of the HMA subtype.[44]

The JNE subtype was characterised by mutations in JAK-STAT and Notch signalling pathways, as well as EBV infection. Accumulating evidence suggests that STAT3 activation leads to constitutive CD30 expression.[12,45] Mutations in Notch signalling pathway are enriched in ALCL, and NOTCH1 and Jagged1 overexpress in $CD30^+$ LPD.[46,47] EBV status is also related to susceptibility and phenotype of $CD30^+$ lymphomas.[48,49] Correspondingly, the gene expression profile of this subtype was characterised by upregulation of immune-associated signalling pathways, including JAK-STAT, Notch, PI3K-AKT, and activation of adaptive immune response. Of note, the patients with the JNE subtype presented worse clinical outcome, similar to those of the JA subtype in $CD30^+$ DLBCL.[9] Regarding therapeutic implications, the JNE subtype demonstrated significantly improved PFS and OS upon the BV treatment, likely due to the immune activation.[50,51] Moreover, the JNE subtype showed increased sensitivity to JAK and PI3K inhibitors. Recent clinical trials have evaluated golidocitinib, a selective JAK1 inhibitor, in treating relapsed or refractory PTCL, demonstrating a higher overall response rate in patients with pSTAT3 $\geq$ 60%.[52,53] The JAK1/2 inhibitor ruxolitinib is also effective in PTCL with activating *JAK* and/or *STAT* mutations.[54] Combination of ruxolitinib and BV shows sustained tumour elimination in murine models of Hodgkin's lymphoma, which is also characterised by CD30 expression and JAK-STAT activation, providing a potential therapeutic approach for investigation in the JNE subtype.[55]

The PCT subtype exhibited aberrations in phosphorylation, chromatin remodelling, and TCR-MHC interaction. Phosphorylation plays a critical role in $CD30^+$ lymphomas, and protein tyrosine phosphatases including *PTPRS*, *PTPRC*, and *PTPN13* were frequently mutated in the PCT subtype, sharing similar characteristics with T3.2.[26] *ARID1A/B*, *ARID2*, *ASXL3*, and *SMARCA2* mutations were also enriched in the PCT subtype, correspondence to the fact that CD30 is regulated by chromatin organizers in ALCL and $CD30^+$ LPD.[56,57] Moreover, abnormalities in MHC molecules are commonly observed in primary mediastinal B-cell lymphoma highly expressing CD30.[58] As for the gene expression profile, chromatin remodelling, ERK signalling pathway, and downstream endoplasmic reticulum activity were upregulated in the PCT subtype. SP8 promoted the FGF signalling pathway in this subtype, contributing to CAF and ECM enrichment in the tumour microenvironment as reported in the solid tumour.[59,60] Regarding therapeutic implications, BV treatment significantly improved PFS and OS in this subtype, likely due to enhanced endoplasmic reticulum activity.[61] Additionally, PD-1 inhibitors may offer therapeutic benefits by reversing the immune evasion.[62] Combining PD-1 inhibitors with BV has demonstrated efficacy in relapsed or refractory primary mediastinal B-cell lymphoma and Hodgkin's lymphoma.[63,64] Clinical trials evaluating similar regimens for patients with relapsed or refractory PTCL are ongoing (NCT04795869 and NCT05313243).

This study has limitations. The molecular subtypes were established by retrospective data, but further validated by the multi-centre validation cohort without significant differences in prognostic features. Secondly, a relatively limited sample size was shown in patients upon BV treatment, due to marketing availability of the drug in China until August 2020.

In conclusion, this multi-omics analysis identified distinct molecular subtypes of $CD30^+$ PTCL. Genetic and microenvironmental alterations contributed to additional biological vulnerabilities, highlighting potential targeted approaches combined with BV treatment for genotype-guided precision medicine in PTCL.

Contributors

Y.-J.H. collected and analysed the data, performed the experiments, and wrote the article. H.-M.J., S.C., T.N., L.F., G.-H.C., F.-L.Z., X.-M.S., F.L., O.B., X.-J.Y, J.S., recruited patients and collected study data. H.-M.Y. and L.D. confirmed the histological diagnoses. Y.-H.H., S.H. and J. X. carried out the sequencing and participated in the validation experiments. Y.-R.Q. was responsible for bioinformatics investigation. P.-P.X and L.W. gave statistical review and verified the underlying data. Z.Y. prepared biological samples. W.-L.Z. conceived the study, directed, and supervised research and wrote the manuscript. All authors read and approved the final version of the manuscript.

Data sharing statement

All sequencing data (including WES and RNA-seq) have been deposited in the GSA-Human database and can be accessed through the following link: https://bigd.big.ac.cn/gsa-human/browse/HRA004246. It is available by contacting the lead contact, Wei-Li Zhao (zhao.weili@yahoo.com), upon request.

Declaration of interests

None of the authors has a relevant conflict of interest.

Acknowledgements

The authors truly thank the clinicians and nurse specialists involved in the care of the patients. We are deeply grateful for the strong support and selfless collaboration from the medical centres of M-HOPES. This study was supported, in part, by research funding from the National Key R&D Program of China (2022YFC2502600), National Natural Science Foundation of China (82130004, 81670176, 82070204, and 82400225), Clinical Research Plan of Shanghai Hospital Development Centre (SHDC2020CR1032B), Shanghai Clinical Research Centre for Cell Therapy (23J41900100), Shanghai Municipal Health Commission (202040400), and China Postdoctoral Science Foundation (2024M752024).

Appendix A. Supplementary data

Supplementary data related to this article can be found at https://doi.org/10.1016/j.ebiom.2025.105693.

References

1 Marchi E, O'Connor OA. The rapidly changing landscape in mature T-cell lymphoma (MTCL) biology and management. *CA Cancer J Clin*. 2020;70(1):47–70.
2 Alaggio R, Amador C, Anagnostopoulos I, et al. The 5th edition of the world health organization classification of haematolymphoid tumours: lymphoid neoplasms. *Leukemia*. 2022;36(7):1720–1748.
3 Campo E, Jaffe ES, Cook JR, et al. The international consensus classification of mature lymphoid neoplasms: a report from the clinical advisory committee. *Blood*. 2022;140(11):1229–1253.
4 Moskowitz AJ, Stuver RN, Horwitz SM. Current and upcoming treatment approaches to common subtypes of PTCL (PTCL, NOS; ALCL; and TFHs). *Blood*. 2024;144(18):1887–1897.
5 Falini B, Pileri S, Pizzolo G, et al. CD30 (Ki-1) molecule: a new cytokine receptor of the tumor necrosis factor receptor superfamily as a tool for diagnosis and immunotherapy. *Blood*. 1995;85(1):1–14.
6 Bossard C, Dobay MP, Parrens M, et al. Immunohistochemistry as a valuable tool to assess CD30 expression in peripheral T-cell lymphomas: high correlation with mRNA levels. *Blood*. 2014;124(19):2983–2986.
7 Karube K, Kakimoto Y, Tonozuka Y, Ohshima K. The expression of CD30 and its clinico-pathologic significance in peripheral T-cell lymphomas. *Expert Rev Hematol*. 2021;14(8):777–787.
8 van der Weyden CA, Pileri SA, Feldman AL, Whisstock J, Prince HM. Understanding CD30 biology and therapeutic targeting: a historical perspective providing insight into future directions. *Blood Cancer J*. 2017;7(9):e603.
9 Huo YJ, Xu PP, Fu D, et al. Molecular heterogeneity of CD30+ diffuse large B-cell lymphoma with prognostic significance and therapeutic implication. *Blood Cancer J*. 2022;12(3):48.
10 Morris SW, Kirstein MN, Valentine MB, et al. Fusion of a kinase gene, ALK, to a nucleolar protein gene, NPM, in non-Hodgkin's lymphoma. *Science*. 1994;263(5151):1281–1284.
11 Velusamy T, Kiel MJ, Sahasrabuddhe AA, et al. A novel recurrent NPM1-TYK2 gene fusion in cutaneous CD30-positive lymphoproliferative disorders. *Blood*. 2014;124(25):3768–3771.
12 Crescenzo R, Abate F, Lasorsa E, et al. Convergent mutations and kinase fusions lead to oncogenic STAT3 activation in anaplastic large cell lymphoma. *Cancer Cell*. 2015;27(4):516–532.
13 Parrilla Castellar ER, Jaffe ES, Said JW, et al. ALK-negative anaplastic large cell lymphoma is a genetically heterogeneous disease with widely disparate clinical outcomes. *Blood*. 2014;124(9):1473–1480.
14 Onaindia A, de Villambrosía SG, Prieto-Torres L, et al. DUSP22-rearranged anaplastic lymphomas are characterized by specific morphological features and a lack of cytotoxic and JAK/STAT surrogate markers. *Haematologica*. 2019;104(4):e158–e162.
15 Bisig B, de Reyniès A, Bonnet C, et al. CD30-positive peripheral T-cell lymphomas share molecular and phenotypic features. *Haematologica*. 2013;98(8):1250–1258.
16 Rodríguez-Pinilla SM, Sánchez ME, Rodríguez J, et al. Loss of TCR-beta F1 and/or EZRIN expression is associated with unfavorable prognosis in nodal peripheral T-cell lymphomas. *Blood Cancer J*. 2013;3(4):e111.
17 Horwitz S, O'Connor OA, Pro B, et al. Brentuximab vedotin with chemotherapy for CD30-positive peripheral T-cell lymphoma (ECHELON-2): a global, double-blind, randomised, phase 3 trial. *Lancet*. 2019;393(10168):229–240.
18 Horwitz S, O'Connor OA, Pro B, et al. The ECHELON-2 Trial: 5-year results of a randomized, phase III study of brentuximab vedotin with chemotherapy for CD30-positive peripheral T-cell lymphoma. *Ann Oncol*. 2022;33(3):288–298.
19 Fanale MA, Horwitz SM, Forero-Torres A, et al. Brentuximab vedotin in the front-line treatment of patients with CD30+ peripheral T-cell lymphomas: results of a phase I study. *J Clin Oncol*. 2014;32(28):3137–3143.
20 Horwitz SM, Advani RH, Bartlett NL, et al. Objective responses in relapsed T-cell lymphomas with single-agent brentuximab vedotin. *Blood*. 2014;123(20):3095–3100.
21 Yi H, Li A, Ouyang B, et al. Clinicopathological and molecular features of indolent natural killer-cell lymphoproliferative disorder of the gastrointestinal tract. *Histopathology*. 2023;82(4):567–575.
22 Basha BM, Bryant SC, Rech KL, et al. Application of a 5 marker panel to the routine diagnosis of peripheral T-cell lymphoma with T-follicular helper phenotype. *Am J Surg Pathol*. 2019;43(9):1282–1290.
23 Leventaki V, Bhattacharyya S, Lim MS. Pathology and genetics of anaplastic large cell lymphoma. *Semin Diagn Pathol*. 2020;37(1):57–71.
24 Dupuis J, Emile JF, Mounier N, et al. Prognostic significance of Epstein-Barr virus in nodal peripheral T-cell lymphoma, unspecified: A Groupe d'Etude des Lymphomes de l'Adulte (GELA) study. *Blood*. 2006;108(13):4163–4169.
25 Chen J, Zhou J, Cheng F, et al. Role of plasma EBV-DNA load and EBER status on newly diagnosed peripheral T-cell lymphoma. *J Cancer Res Clin Oncol*. 2024;150(4):181.
26 Huang YH, Qiu YR, Zhang QL, et al. Genomic and transcriptomic profiling of peripheral T cell lymphoma reveals distinct molecular and microenvironment subtypes. *Cell Rep Med*. 2024;101416.
27 Dobin A, Davis CA, Schlesinger F, et al. STAR: ultrafast universal RNA-seq aligner. *Bioinformatics*. 2013;29(1):15–21.
28 Anders S, Pyl PT, Huber W. HTSeq–a Python framework to work with high-throughput sequencing data. *Bioinformatics*. 2015;31(2):166–169.
29 Bray NL, Pimentel H, Melsted P, Pachter L. Near-optimal probabilistic RNA-seq quantification. *Nat Biotechnol*. 2016;34(5):525–527.
30 Kotlov N, Bagaev A, Revuelta MV, et al. Clinical and biological subtypes of B-cell lymphoma revealed by microenvironmental signatures. *Cancer Discov*. 2021;11(6):1468–1489.
31 Subramanian A, Tamayo P, Mootha VK, et al. Gene set enrichment analysis: a knowledge-based approach for interpreting genome-wide expression profiles. *Proc Natl Acad Sci U S A*. 2005;102(43):15545–15550.
32 Iqbal J, Wright G, Wang C, et al. Gene expression signatures delineate biological and prognostic subgroups in peripheral T-cell lymphoma. *Blood*. 2014;123(19):2915–2923.
33 Hänzelmann S, Castelo R, Guinney J. GSVA: gene set variation analysis for microarray and RNA-seq data. *BMC Bioinformatics*. 2013;14:7.
34 Basu A, Bodycombe NE, Cheah JH, et al. An interactive resource to identify cancer genetic and lineage dependencies targeted by small molecules. *Cell*. 2013;154(5):1151–1161.
35 Iqbal J, Inghirami G, Chan WC. New insights into the biology of T-cell lymphomas. *Blood*. 2024;144(18):1873–1886.
36 Xiao C, Fan T, Tian H, et al. H3K36 trimethylation-mediated biological functions in cancer. *Clin Epigenetics*. 2021;13(1):199.
37 Zhong LH, Wu ZD, Wang JC, et al. Molecular profiling of Chinese systemic anaplastic large cell lymphoma patients: novel evidence of genetic heterogeneity. *Ann Transl Med*. 2021;9(2):128.
38 Abdulla FR, Zhang W, Wu X, et al. Genomic analysis of cutaneous CD30-positive lymphoproliferative disorders. *JID Innov*. 2022;2(1):100068.
39 Wang H, Guo M, Wei H, Chen Y. Targeting p53 pathways: mechanisms, structures, and advances in therapy. *Signal Transduct Target Ther*. 2023;8(1):92.
40 Ruan J, Moskowitz A, Mehta-Shah N, et al. Multicenter phase 2 study of oral azacitidine (CC-486) plus CHOP as initial treatment for PTCL. *Blood*. 2023;141(18):2194–2205.
41 Wong J, Gruber E, Maher B, et al. Integrated clinical and genomic evaluation of guadecitabine (SGI-110) in peripheral T-cell lymphoma. *Leukemia*. 2022;36(6):1654–1665.
42 Ji MM, Huang YH, Huang JY, et al. Histone modifier gene mutations in peripheral T-cell lymphoma not otherwise specified. *Haematologica*. 2018;103(4):679–687.
43 Camus V, Thieblemont C, Gaulard P, et al. Romidepsin plus cyclophosphamide, doxorubicin, vincristine, and prednisone versus

cyclophosphamide, doxorubicin, vincristine, and prednisone in patients with previously untreated peripheral T-cell lymphoma: final analysis of the ro-CHOP trial. *J Clin Oncol*. 2024;42(14):1612–1618.
44 Tonozuka Y, Tanaka H, Nomura K, Sakaguchi K, Soeda J, Kakimoto Y. The combination of brentuximab vedotin and chidamide synergistically suppresses the proliferation of T-cell lymphoma cells through the enhancement of apoptosis. *Cancer Chemother Pharmacol*. 2024;93(2):137–149.
45 Chen J, Zhang Y, Petrus MN, et al. Cytokine receptor signaling is required for the survival of ALK- anaplastic large cell lymphoma, even in the presence of JAK1/STAT3 mutations. *Proc Natl Acad Sci U S A*. 2017;114(15):3975–3980.
46 Kamstrup MR, Ralfkiaer E, Skovgaard GL, Gniadecki R. Potential involvement of Notch 1 signalling in the pathogenesis of primary cutaneous CD30-positive lymphoproliferative disorders. *Br J Dermatol*. 2008;158(4):747–753.
47 Gao X, Wang C, Abdelrahman S, et al. Notch signaling promotes mature T-cell lymphomagenesis. *Cancer Res*. 2022;82(20):3763–3773.
48 Wai CMM, Chen S, Phyu T, et al. Immune pathway upregulation and lower genomic instability distinguish EBV-positive nodal T/NK-cell lymphoma from ENKTL and PTCL-NOS. *Haematologica*. 2022;107(8):1864–1879.
49 Yu F, Wang J, Ke Z, et al. EBV-positive nodal T-cell and NK-cell lymphoma: a study of 26 cases including a subset with strong CD30 expression mimicking anaplastic large cell lymphoma. *Am J Surg Pathol*. 2024;48(4):406–416.
50 Clynes RA, Towers TL, Presta LG, Ravetch JV. Inhibitory Fc receptors modulate in vivo cytotoxicity against tumor targets. *Nat Med*. 2000;6(4):443–446.
51 Müller P, Martin K, Theurich S, et al. Microtubule-depolymerizing agents used in antibody-drug conjugates induce antitumor immunity by stimulation of dendritic cells. *Cancer Immunol Res*. 2014;2(8):741–755.
52 Song Y, Yoon DH, Yang H, et al. Phase I dose escalation and expansion study of golidocitinib, a highly selective JAK1 inhibitor, in relapsed or refractory peripheral T-cell lymphomas. *Ann Oncol*. 2023;34(11):1055–1063.
53 Song Y, Malpica L, Cai Q, et al. Golidocitinib, a selective JAK1 tyrosine-kinase inhibitor, in patients with refractory or relapsed peripheral T-cell lymphoma (JACKPOT8 Part B): a single-arm, multinational, phase 2 study. *Lancet Oncol*. 2024;25(1):117–125.
54 Moskowitz AJ, Ghione P, Jacobsen E, et al. A phase 2 biomarker-driven study of ruxolitinib demonstrates effectiveness of JAK/STAT targeting in T-cell lymphomas. *Blood*. 2021;138(26):2828–2837.
55 Ju W, Zhang M, Wilson KM, et al. Augmented efficacy of brentuximab vedotin combined with ruxolitinib and/or Navitoclax in a murine model of human Hodgkin's lymphoma. *Proc Natl Acad Sci U S A*. 2016;113(6):1624–1629.
56 Wang Y, Gu X, Zhang G, et al. SATB1 overexpression promotes malignant T-cell proliferation in cutaneous CD30+ lymphoproliferative disease by repressing p21. *Blood*. 2014;123(22):3452–3461.
57 Luchtel RA, Zimmermann MT, Hu G, et al. Recurrent MSC (E116K) mutations in ALK-negative anaplastic large cell lymphoma. *Blood*. 2019;133(26):2776–2789.
58 Lees C, Keane C, Gandhi MK, Gunawardana J. Biology and therapy of primary mediastinal B-cell lymphoma: current status and future directions. *Br J Haematol*. 2019;185(1):25–41.
59 Wagner AE, Schwarzmayr T, Häberle B, et al. SP8 promotes an aggressive phenotype in hepatoblastoma via FGF8 activation. *Cancers (Basel)*. 2020;12(8).
60 Chen Y, McAndrews KM, Kalluri R. Clinical and therapeutic relevance of cancer-associated fibroblasts. *Nat Rev Clin Oncol*. 2021;18(12):792–804.
61 Heiser RA, Cao AT, Zeng W, et al. Brentuximab vedotin-driven microtubule disruption results in endoplasmic reticulum stress leading to immunogenic cell death and antitumor immunity. *Mol Cancer Ther*. 2024;23(1):68–83.
62 Li J, Wu C, Hu H, et al. Remodeling of the immune and stromal cell compartment by PD-1 blockade in mismatch repair-deficient colorectal cancer. *Cancer Cell*. 2023;41(6):1152–1169.e7.
63 Zinzani PL, Santoro A, Gritti G, et al. Nivolumab combined with brentuximab vedotin for relapsed/refractory primary mediastinal large B-cell lymphoma: efficacy and safety from the phase II CheckMate 436 study. *J Clin Oncol*. 2019;37(33):3081–3089.
64 Advani RH, Moskowitz AJ, Bartlett NL, et al. Brentuximab vedotin in combination with nivolumab in relapsed or refractory Hodgkin lymphoma: 3-year study results. *Blood*. 2021;138(6):427–438.